# *Jumping droplet condensation in internal convective vapor flow*

# Jumping Droplet Condensation in Internal Convective Vapor Flow

Dion S. Antao[†], Kyle L. Wilke, Jean H. Sack, Zhenyuan Xu, Daniel J. Preston[‡] and Evelyn N. Wang[*]

Department of Mechanical Engineering, Massachusetts Institute of Technology, Cambridge, MA 02139, USA

**Abstract**

Condensation is an important process in the Rankine cycle that significantly affects overall efficiency. Condensate typically forms a liquid film due to the high surface energy of industrial condenser materials; by engineering the condenser surface with a superhydrophobic layer, however, we can increase condensation heat transfer by an order of magnitude with the jumping droplet mode of condensation. While the basic phenomenon of jumping droplet condensation has been explored in depth, its effects on heat transfer and pressure drop in *confined* vapor flow *inside* a condenser tube, as in power plant condensers, have not been considered. Here, we report an experimental study of internal forced convective condensation with hydrophilic, hydrophobic, and superhydrophobic surfaces to study condensation in the filmwise, dropwise, and jumping droplet modes, respectively. The condenser tube samples were tested in a closed system internal flow condensation setup, and the heat transfer and pressure drop behavior were characterized over various operating conditions. In the jumping droplet mode, the heat transfer coefficient was highest at lower condensation heat flux and condenser surface subcooling, and a transition to the flooded mode at higher subcooling resulted in a heat transfer coefficient comparable to filmwise condensation. For dropwise condensation in the hydrophobic tube, the condensation heat transfer coefficient increased with the vapor velocity, similar to observations in past work. In addition to a large heat transfer coefficient, the pressure drop with the superhydrophobic tube samples was the lowest. These experimental results demonstrate the viability of harnessing the jumping droplet mode of condensation to enhance heat transfer and reduce pressure drop for internal forced convective flow condensation in industrial condensers.

*Keywords*: Jumping droplet condensation, internal convective condensation, vapor shear

Manuscript submitted to the *International Journal of Heat and Mass Transfer*, May, 2020

[†]Current address: Department of Mechanical Engineering, Texas A&M University

[‡]Current address: Department of Mechanical Engineering, Rice University

[*]Corresponding author, e-mail: enwang@mit.edu

## 1. Introduction

Water vapor condensation is a key process in electric power generation, and over 50% of the total electric energy production systems in the United States (>4 trillion kWh) use a steam-based Rankine power cycle with a condenser [1]. Enhancing condensation heat transfer results in the highest potential increase in net cycle efficiency [2], and enables cost effective power plant setup and environmentally sustainable operation *via* a reduction in energy and fresh water consumption [3-5].

Two main modes of condensation for water have been researched for many decades and they are primarily dependent on the wettability of the condenser surface: filmwise and dropwise condensation. In filmwise condensation, the condensing water vapor forms a thin liquid film (>10-100 μm) on a highly wetting or hydrophilic condenser surface (*e.g.*, metals or metal oxides). The low thermal conductivity of the condensate film raises the barrier to condensation, resulting in low condensation heat transfer coefficients [6]. On hydrophobic materials, the condensing water vapor forms discrete droplets that are shed from the surface faster than filmwise condensation, and cleans the condenser surface for new condensate nucleation events [7]. This rapid shedding of the droplets leads to a higher heat transfer coefficient than filmwise condensation. For traditional dropwise condensation, the droplets grow to the capillary length scale (≈3 mm for water) before gravitational forces overcome surface tension forces and drive droplet departure. When the condenser surface is superhydrophobic, *i.e.*, contact angle $\theta$ >150° and contact angle hysteresis $\Delta\theta$ <10°, and has favorable surface structure length scales [8], the condensing vapor can form small droplets that self-eject or *jump* from the surface upon coalescence with each other [9, 10]. This mode of condensation is referred to jumping droplet condensation and the condensation heat transfer coefficient can be greater than traditional dropwise condensation due to the smaller droplet sizes at their time of departure from the surface. The droplet departure mechanism after coalescence is due to the partial conversion of the excess surface energy (decrease in total surface area when two droplets merge to form one) to kinetic energy [11-16].

Jumping droplet condensation was first reported with condensing mercury [17], however recent work with water as the working fluid [9, 10, 13, 18-20] has demonstrated a wide range of applications and quantified heat transfer enhancements [21, 22]. Jumping droplet condensation on condenser surfaces in a quiescent or natural convective water vapor ambient have shown enhancements in heat transfer coefficient over dropwise condensation up to 100% [19, 23, 24]. However, until recently, a key limitation to jumping droplet condensation has been the

transition to the flooded mode where heat transfer is degraded. The flooded mode typically occurs at low surface subcooling (*i.e.*, the temperature difference between the vapor and condenser surface) of ≈2-5 K and is irreversible during condensation. At these critical subcooling levels, the condensate nucleation density is sufficiently high such that the distance between the nucleating droplets approaches the superhydrophobic surface structure length scale. This causes the droplets to be pinned to the surface structures and increases the droplet departure size. Wen *et al.* [25] recently demonstrated that with optimal design of the nanostructures used to create superhydrophobic surfaces, this nucleation density mediated flooding can be delayed to higher surface subcooling.

Currently, there are few studies characterizing the applicability of jumping droplet condensation in the presence of vapor shear found in internal flows [26, 27]. There are also few experimental studies for traditional dropwise condensation (hydrophobic surfaces) in the presence of internal vapor flows that characterize vapor shear effects [28, 29]. In these studies, dropwise condensation inside tubes was studied under air-cooled conditions, and hence the enhancement over filmwise condensation was limited to 1.5-2× [28]. The work in [29] also reported visualizations of the internal dropwise condensation process for circular Pyrex tubes, and over longer sections of the condenser tube, the effects of gravity and droplet shedding upstream led to the formation of condensate flow *streams* instead of discrete droplets. This latter effect may be overcome by harnessing the jumping droplet mode [26, 27].

In this work, we focus on investigating the effect of confined vapor flows on jumping droplet heat transfer and pressure drop. In particular, we are interested in applications for large scale thermoelectric power generation facility condensers [27]. Accordingly, we synthesized superhydrophobic condenser tube samples in a scalable manner to promote jumping droplets and tested them in a custom built flow setup. With this setup, we characterized heat transfer and pressure drop performance of hydrophilic, hydrophobic and superhydrophobic condenser tube samples at industrially relevant conditions, *i.e.*, vapor temperature ≈60 °C, vapor velocity ≈20-40 m/s, and condensation heat flux ≈40 kW/m$^2$ or higher. These test conditions are typical for air-cooled condenser (ACC) used in coal-fired power plants [3].

## 2. Experimental Setup and Methods

We describe the experimental setup, the condenser tube sample synthesis/fabrication, experimental procedure, and data analysis and reduction here. Further information on a sample

data set for steady state operation and on uncertainty estimation procedures are presented in the Appendix.

2.1. Experimental setup

We performed experiments in a custom built instrumented test setup (schematically shown in Figure 1a) which included a vapor source boiler, heat exchanger and test section (condenser tube sample), a collection/water reservoir, and a refrigerated water chiller (K4, ATC). The boiler is a cylindrical canister of volume ≈5.5 L with electric heaters capable of delivering 5000 W. This heater power was regulated with variable AC transformers and PID controllers (CN7823, Omega Engineering), and the temperature of the water and vapor inside the boiler were monitored with thermocouples. The pressure of the boiler was monitored using a pressure transducer (PX409, Omega Engineering). All thermocouples used in the setup were 0.159 cm diameter J-type stainless steel sheath probes.

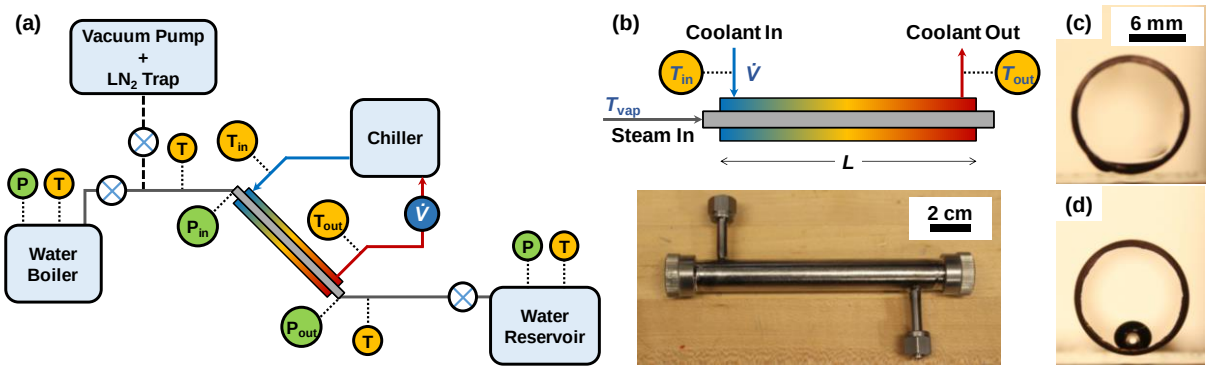


**Figure 1**: (a) Schematic of the experimental test setup showing key measurements (pressure $P$, temperature $T$, and volumetric flowrate $\dot{V}$). The dotted lines show measurements made on the fluid inside the system, the dashed line indicates the evacuation line to the vacuum pump, and the solid gray line indicates the steam flow path from the boiler through the test section to the reservoir. (b) Schematic and image of the shell-and-tube heat exchanger test section. Cross-section images of water droplets in (c) hydrophilic and (d) superhydrophobic condenser tube samples.

Every condenser sample tested was a copper tube of outer ($d_{OD}$) and inner ($d_{ID}$) diameters ≈1.27 cm and ≈1.15 cm, respectively, and length ($L_{tube}$) ≈19 cm. The condenser was inserted into a custom fabricated stainless steel shell-and-tube water jacket heat exchanger (Figure 1b) of inner diameter 1.32 cm and length ≈16 cm (note that the active heat transfer length $L$ was ≈11.5 cm), and was oriented at ≈40° to the horizontal for all experiments. Vapor flow and condensation occurred on the inside of the condenser tube sample and the coolant (water)

flowed through the annulus of the shell. Thermocouples and pressure transducers (PX409, Omega Engineering) were used to monitor the vapor inlet and outlet temperatures and pressures, respectively. The small gap of the annulus (≈500 μm) enabled high convective heat transfer coefficients at low coolant flowrates, minimizing the coolant flowrate measurement uncertainty. The refrigerated chiller circulated the coolant through an external flow loop connected to the heat exchanger, and the coolant temperature into and out of the heat exchanger were monitored with thermocouples. The flowrate of the coolant was measured with a laminar-flow liquid flowmeter (L-10LPM-D, Alicat Scientific).

The vapor-condensate mixture at the outlet of the test section was directed into the water reservoir where the remaining vapor was condensed to liquid. The temperature set point of water in the reservoir was maintained by a separate refrigerated chiller (Isotemp R35, Fisher Scientific). The reservoir was also instrumented with thermocouples, external heaters and a pressure transducer (PX409, Omega Engineering) to monitor and control the fluid conditions.

All instrumentation *i.e.*, pressure transducers and thermocouples, were connected to data acquisition cards (PCI-6289 and 9214, National Instruments), and the data was captured using a LabVIEW interface. The thermocouples used in the setup were all calibrated in a water-bath (RE207, Lauda) with a resistance temperature detector (RTD-810, Omega Engineering). Since experiments were performed for water condensing at temperatures below 100 °C, the boiler, connecting vapor lines and collection reservoir were all leak tested with a helium leak detector (ASM 142, Adixen) under vacuum conditions. The measured leak rate ($<5\times10^{-11}$ Pa·m$^3$/s) was sufficiently low to ensure minimal effects from non-condensable gases during experiments.

2.2. Condenser tube samples fabrication/synthesis

Copper was used as the tube material in all tests, and three different types of surfaces were exposed to the vapor flow: native cuprous oxide $Cu_2O$ (Figure 1c), hydrophobic coating (<0.5 μm thick, NEI Corp), and cupric oxide (CuO) nanostructures with conformal hydrophobic coating (<0.05 μm thick, P2i, Figure 1d). With these different surfaces, we measured condensation heat transfer rates and pressure drop through the tube sample for the filmwise, dropwise and jumping droplet modes. We briefly describe the procedure for each tube sample synthesis/preparation, and prior to all synthesis procedures, we solvent cleaned the samples with acetone (in an ultrasonic bath), methanol, isopropanol and deionized (DI) water.

To promote complete wetting of the copper tube for filmwise condensation and ensure minimal contamination of the sample from airborne hydrocarbons [30], we created a layer of cuprous

oxide ($Cu_2O$) on the copper tube *via* wet oxidation. Due to the aspect ratio ($d_{ID}/L_{tube}$) of the test sample, wet oxidation offered a scalable alternative to ensure a pristine surface prior to experimentation compared to plasma cleaning. We facilitated the growth of the oxide layer by stripping the native oxide using 2.0 M hydrochloric acid (HCl) solution, rinsing the tube sample with DI water, and immersing it in hydrogen peroxide ($H_2O_2$) for 20 minutes. After immersion in $H_2O_2$, we rinsed the sample in DI water, dried it with compressed air and inserted it into the test section (shell-and-tube heat exchanger). The samples retained their hydrophilicity, *i.e.*, the internal walls of the tube instantly wet when a water droplet contacted the surface, after testing ≈8-10 hours.

For the dropwise condensation tests, we used a tube sample coated internally with a polymer coating (SuperCN) by NEI Corp. To promote jumping droplet condensation, we scalably synthesized cupric oxide nanostructures (CuO) on the internal surface of the tube samples using the wet chemistry detailed by Miljkovic *et al.* [19], and a thin conformal hydrophobic polymer coating was applied *via* PECVD by P2i Ltd. CuO nanostructures with thin (<0.05 μm) conformal hydrophobic coatings have been shown to promote jumping droplet condensation with highly mobile droplet morphologies, due to the favorable nanostructure geometry and the nucleation densities achieved with the coatings [8, 19, 31]. We did not modify or clean the internal surfaces of the tubes after coatings were applied by NEI Corp and P2i Ltd.

### 2.3. Measurement and experimental procedure

We followed a rigorous and consistent experimental procedure for all the samples tested and in this sub-section we briefly describe the key steps followed. For every experimental run (*i.e.*, a different tube sample), we filled the boiler with pure DI water (34877-M HPLC-Plus, Sigma Aldrich) and drained the reservoir (to <50 mL of water). Non-condensable gasses (NCGs) in the vapor/condensate lines of the test setup or dissolved in the water in the boiler or collection reservoir can lead to a degradation of the measured heat transfer rates [7, 32]. To remove dissolved NCGs, we thoroughly degassed both the boiler and the reservoir. The degassing procedure involved a combination of boiling the water in the boiler and reservoir and pulling vacuum on the vapor space in each component. The vapor space was exposed to vacuum multiple times while the water was boiling at atmospheric pressure (measured liquid temperature >100 °C). This procedure was performed one day prior to testing to ensure that the water in both the boiler and reservoir were degassed. We verified the degassed state of the water immediately before the experiments by comparing the measured pressure in the vapor

space with the saturation vapor pressure corresponding to the temperature of the vapor space, and ensuring that they were within the measurement uncertainty.

After inserting the tube samples into the test section, we pulled vacuum on the flow lines exposed to vapor, *i.e.*, the lines connecting the boiler to the test section and the test section to the reservoir, to purge the lines of any NCGs. A combination of the vacuum pump (2010SD, Adixen) and liquid nitrogen ($LN_2$) cold trap ensured that the minimum pressure achieved as measured by the vacuum transducer (925, MKS Instruments) was $10^{-3}$ Pa, which was maintained until the experiments were started. The $LN_2$ trap acted as a cryopump to help achieve lower pressures than the rotary vane pump alone.

During condensation experiments, we maintained a constant coolant flowrate $\dot{V}$ (2.2±0.3 LPM), and varied the coolant inlet temperature ($T_{in}$) to achieve different combinations of condensation heat transfer rates and surface subcooling. We varied the opening of the metering valve (SS-8BG, Swagelok) connecting the boiler and the vapor line to control the vapor flowrate and temperature ($T_{vap}$) at the inlet of the tube sample depending on the $T_{in}$ condition. We maintained a constant vapor temperature at the inlet to the test section ($T_{vap}$) for all experiments ≈60 °C and varied $T_{in}$ from 59.5 °C to 40 °C. This temperature of 60 °C was chosen since it is a typical vapor condensation temperature in industrial ACCs [3]. The vapor line connecting the boiler to the test section was maintained at 60 °C using rope heaters and a PID controller. Similarly, the line connecting the test section and the reservoir, and the fluid in the reservoir were maintained at ≈30 °C. The test section was wrapped in foam insulation (thickness ≈4-5 cm) to ensure that the sensible heat rise measured in the heat exchanger ($\Delta T_{flow} = T_{out} - T_{in}$) was due to condensation heat transfer. Before the first condensation measurement, we collected and stored data to provide zero/datum values to correct for any measurement offsets during testing (primarily for $\Delta T_{flow}$, $\dot{V}$ and $\Delta P_{vap}$).

A typical experiment involved setting the coolant loop temperature and opening the metering valve until the vapor temperature at the inlet of the test section was ≈60 °C. This initial transient operation required the PID controllers for the boiler to be auto-tuned such that the optimum P, I and D coefficients could be achieved to maintain steady operation where the heat input into the boiler matched the total heat lost in the setup including the heat of condensation removed by the coolant loop. Steady state operation, *i.e.*, constant temperature/pressure in the boiler, vapor lines and reservoir, and the temperatures and coolant flowrate in the test section, was achieved in ≈8-10 min. We then acquired data for 4 minutes at an acquisition rate of 10 Hz

before closing the metering valve, changing the coolant inlet temperature, and repeating the procedure at a different $T_{in}$.

2.4. Data analysis and reduction

We estimated the condensation heat flux by measuring the sensible heat rise in the heat exchanger and flowrate of the coolant through the heat exchanger:

$$q'' = \frac{\dot{m}_{coolant} \cdot c_p}{A_i} \left( \Delta T_{flow} \right) \tag{1}$$

where $q''$ is the average heat flux, $\dot{m}$ is the mass flowrate of the coolant ($\dot{m}_{coolant} = \rho_{coolant} \cdot \dot{V}$, $\rho_{coolant}$ is the coolant density), $c_p$ is the specific heat capacity of the coolant evaluated at the average coolant temperature, $A_i$ is the tube internal surface area where condensation occurs. All the data analysis is performed for steady state data averaged over 3 minutes. An example steady state data set is shown in Appendix A.

To estimate the condensation heat transfer coefficient $h_{cond}$, we calculated the overall heat transfer coefficient $\bar{U}$ for the heat exchanger as:

$$\bar{U} = \frac{\dot{m}_{coolant} \cdot c_p}{\Delta T_{LM} \cdot A_i} \left( \Delta T_{flow} \right) \tag{2}$$

where $\Delta T_{LM}$ is the log mean temperature difference defined as follows:

$$\Delta T_{LM} = \frac{\left( T_{vap} - T_{in} \right) - \left( T_{vap} - T_{out} \right)}{\ln \left( \frac{T_{vap} - T_{in}}{T_{vap} - T_{out}} \right)} \tag{3}$$

$T_{vap}$ is the vapor temperature at the inlet to the tube test section and $T_{in}$ and $T_{out}$ are the coolant inlet and outlet temperatures.

The condensation heat transfer coefficient was obtained using a one-dimensional thermal resistance network for heat transfer from the condensate to the coolant through the tube wall:

$$\begin{aligned} \frac{1}{A_i \cdot \bar{U}} &= \frac{1}{A_o \cdot h_{convection}} + \frac{1}{A_i \cdot h_{condensation}} + \frac{\ln \left( d_{OD} / d_{ID} \right)}{2\pi \cdot L \cdot k_{tube}} \\ h_{condensation} &= \left[ \frac{1}{\bar{U}} - \frac{A_i}{A_o \cdot h_{convection}} - \frac{A_i \cdot \ln \left( d_{OD} / d_{ID} \right)}{2\pi \cdot L \cdot k_{tube}} \right]^{-1} \end{aligned} \tag{4}$$

where $A_o$ is the outer surface area of the tube in contact with the coolant, $L$ is the tube length over which heat transfer occurs (≈11.5 cm), $k_{tube}$ is the tube material thermal conductivity, and $h_{convection}$ is the coolant convective heat transfer coefficient (Gnielinski correlation [33]):

$$h_{\text{convection}} = \frac{k_{\text{water}}}{d_{\text{annulus}}}\left(\frac{(f/8)(\text{Re}-1000)\cdot\text{Pr}}{1+12.7(f/8)^{1/2}\left(\text{Pr}^{2/3}-1\right)}\right) \qquad (5)$$

$$f = \left(0.79\cdot\ln(\text{Re})-1.64\right)^{-2} \qquad \text{Re} = \frac{\rho_{\text{coolant}}\cdot v_{\text{coolant}}\cdot d_{\text{annulus}}}{\mu_{\text{coolant}}}$$

where $k_{\text{water}}$ is the coolant thermal conductivity, $f$ is the friction factor, Re and Pr are the Reynolds and Prandtl numbers respectively, $\mu_{\text{coolant}}$ is the coolant viscosity, $d_{\text{annulus}}$ is the heat exchanger annulus hydraulic diameter and $v_{\text{coolant}}$ is the coolant velocity in the annulus of the heat exchanger.

The steam-side pressure drop through the tube was measured over the length of the entire test section (≈19 cm), using two pressure transducers:

$$\Delta P_{\text{vap}} = P_{\text{in}} - P_{\text{out}} \qquad (6)$$

where $P_{\text{in}}$ and $P_{\text{out}}$ are the inlet and outlet pressures of the vapor flowing through the tube.

The steam-side velocity within the test section was estimated (choked flow conditions) based on conditions in the boiler and measurements along the vapor lines connecting the boiler and the test section:

$$v_{\text{steam}} = 0.0002\left(\frac{C_{\text{v}}}{A_1}\sqrt{\frac{\rho_{\text{air}}}{\rho_{\text{vap}}}}\sqrt{\left(T_{\text{boiler-vap}}+273.15\right)}\right) \qquad (7)$$

where $C_{\text{v}}$ is the flow coefficient of the orifice (SS-8BG, Swagelok), $T_{\text{boiler-vap}}$ is the temperature of the vapor in the boiler and $\rho_{\text{vap}}$ and $\rho_{\text{air}}$ are the densities of vapor and air.

Finally, we also estimated the vapor quality $x$ at the outlet of the test section based on the steam velocity estimation and an energy balance in the condenser:

$$x = 1 - \frac{q''\cdot A_1}{\dot{m}_{\text{vap-in}}\cdot h_{\text{fg}}}$$
$$\dot{m}_{\text{vap-in}} = \rho_{\text{vap}}\cdot v_{\text{steam}}\cdot\left(\frac{\pi}{4}d_{\text{ID}}^2\right) \qquad (8)$$

where $\dot{m}_{\text{vap-in}}$ is the inlet steam mass flowrate, $q''$ is the condensation heat flux and $h_{\text{fg}}$ is the latent heat of vaporization of the water.

In addition to calculating the heat transfer and pressure drop characteristics during the various modes of condensation, we also assessed the uncertainty in our measurements. The analysis

for all uncertainty can be found in Appendix B, and all uncertainty bars in the data reported here were from this uncertainty analysis.

### 3. Results and Discussion

We measured condensation heat flux data for a wide range of surface subcooling on each of the tube samples tested, and the condensation heat flux is plotted in Figure 2a as a function of the log mean temperature difference in the test section. The expected modes of condensation were filmwise, traditional dropwise, and jumping droplet on the hydrophilic, hydrophobic and superhydrophobic surfaces, respectively . At low values of $\Delta T_{LM}$ (Figure 2b) the dominant thermal resistance was from the coolant convection outside the tube sample, hence the measured data from the different modes were clustered together and appeared to have the same slope (within measurement uncertainty).

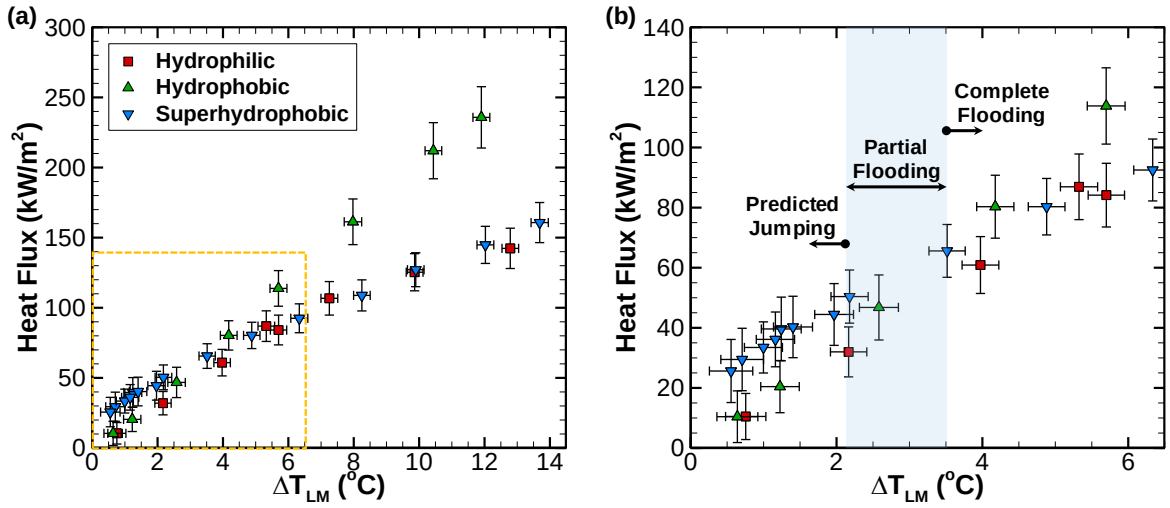


**Figure 2**: Measurements of condensation heat fluxes in the filmwise (hydrophilic, $Cu_2O$), traditional dropwise (hydrophobic, SuperCN coating), and the jumping droplet (superhydrophobic, P2i coating on CuO nanostructures) modes for different heat exchanger log mean temperature differences. The plot in (b) highlights the low $\Delta T_{LM}$ and low $q$" measurements in (a) (dashed box area) indicating the expected jumping droplet operating regime and the transitions to the flooding mode where there are highly pinned droplets on the surface, hindering heat transfer [19].

As the surface subcooling increased, the rate of condensation increased, however as seen in Figure 2a, there was a change in the slope for $q$" *v/s* $\Delta T_{LM}$ for the hydrophilic and superhydrophobic surfaces. In the case of the hydrophobic surface which promoted traditional dropwise condensation, the gravitationally and shear driven droplet shedding sustained

continuous surface cleaning for new condensation nucleation events. This was expected to occur until defects in the hydrophobic coating caused excessive droplet pinning, or when the surface subcooling (or supersaturation, $S$) was sufficiently high to increase the nucleation density to the point of condenser surface flooding. The supersaturation for condensation is typically defined as the ratio of the vapor pressure to the saturation pressure at the condenser surface temperature. Due to this steady droplet shedding behavior, a near-linear relation in the $q''$ *v/s* $\Delta T_{LM}$ data was expected as the subcooling increased. For the hydrophilic surface, we attributed the change in slope with increasing subcooling to the increase in the condensate film thickness inside the tube. This would increase the thermal resistance to heat transfer on the condensation-side and hence reduce the overall heat transfer coefficient $\approx q''/\Delta T_{LM}$.

The change in the slope for the case of the superhydrophobic surface was attributed to a change in the condensation mode from the efficient jumping droplet mode to the flooding mode where highly-pinned Wenzel droplets were on the condenser surface. As stated earlier, this typically occurs above some critical supersaturation (or condenser subcooling) identified by Miljkovic *et al.* [19] to be $S_{cr} \approx 1.12$ for CuO nanostructures with a hydrophobic coating. From classical nucleation theory, nucleation density is primarily determined by the supersaturation with only a weak dependence on the condensation temperature for the CuO and hydrophobic coating material [34]. Hence, we applied the same $S_{cr} \approx 1.12$ criterion for our experiments at $T_{cond} \approx 50\text{-}60$ °C (compared to $T_{cond} \approx 10\text{-}20$ °C in [19], see Appendix C for additional information). Given that the coolant temperature increased along the length of the test section, the local supersaturation must satisfy the condition of $S_{local} < S_{cr}$ for condensation to be in the jumping droplet mode. Hence in Figure 2b (corresponding to the dashed box in Figure 2a), we identified three regions on the $q''$ *v/s* $\Delta T_{LM}$ curve for the superhydrophobic surface: predicted jumping, partial flooding and complete flooding regions. Here, $S_{local}$ was predicted using a 1D thermal resistance model and a value of $S_{cr} \approx 1.12$ was used (Appendix C). For the predicted jumping region, $S_{local} < S_{cr}$ in the entire tube sample, and in the complete flooding region, $S_{local} > S_{cr}$ for the entire tube sample. In the partial flooding region, $S_{local} > S_{cr}$ at the inlet, however, at the outlet, $S_{local} < S_{cr}$. This predicted transition from the jumping droplet mode to full/complete flooding (shaded region in Figure 2b) correlated well with the changing slope of the $q''$ *v/s* $\Delta T_{LM}$ data; high slope ($\Delta T_{LM} < 2$ °C) to low slope ($\Delta T_{LM} < 3.5$ °C).

The measurements presented in Figure 2 are for the total heat transfer from the vapor flow inside the tube sample to the coolant flow outside the tube. To characterize the heat transfer coefficient solely due to condensation ($h_{condensation}$), we used eq. 4 which models a 1D thermal

resistance network. The condensation heat transfer coefficient (HTC) is plotted in Figure 3 for the different modes identified above and at different condensation heat flux values.

Filmwise condensation (hydrophilic surface) had the lowest average HTC ≈23 ± 7 kW/m$^2$·K. Increasing the surface subcooling (and condensation heat flux) increased the condensate film thickness and resulted in a decreased HTC (Figure 3). For the jumping droplet mode on the superhydrophobic CuO surface, the average condensation HTC was ≈66 ± 4 kW/m$^2$·K. However, as the surface transitioned to the flooded mode, the average HTC was ≈26 ± 8 kW/m$^2$·K due to pinned droplets of irregular size [19] and decreased droplet departure rates. Similar to filmwise condensation, as the surface subcooling was increased, the HTC for the flooded mode decreased as the surface flooded due to the coalescence of droplets pinned to the condenser surface. During dropwise condensation on the hydrophobic surface, the average HTC was ≈57 ± 9 kW/m$^2$·K. Here, the HTC increased with heat flux in contrast to the behavior during filmwise and jumping droplet condensation.

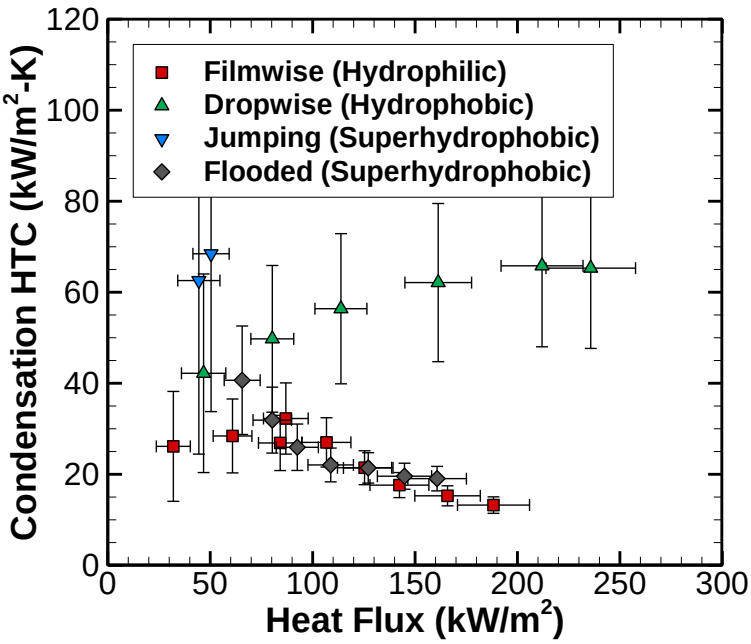


**Figure 3**: Estimated condensation heat transfer coefficient (HTC) from measurements and a 1D thermal resistance network for the different modes of condensation on the hydrophilic, hydrophobic and superhydrophobic surfaces.

The increasing HTC for dropwise condensation with increasing heat flux may be attributed to the increased steam velocity and subcooling at higher heat flux. In the experiments reported here, the vapor velocity at the entrance to the test section was dependent on the valve opening size ($\propto C_v$) and the temperature in the boiler. A larger valve opening and $C_v$ was required to

maintain a constant $T_{vap}$ at the inlet of the test section when the surface subcooling was increased. This resulted in increased inlet vapor velocity at the entrance of the test section at higher condensation heat fluxes (Figure 4a). Droplets on the hydrophobic surface were more mobile in the presence of vapor shear, compared to the film in filmwise condensation and the pinned droplets in the flooded mode on the superhydrophobic surface. This behavior (increased HTC with increased vapor velocity) was also observed by Torresin *et al.* [35] for internal convective dropwise condensation (non-jumping mode) on superhydrophobic copper surfaces. Overall in our experiments, the highest condensation heat transfer coefficients were observed for dropwise condensation at high vapor velocity and jumping droplet condensation at low supersaturation.

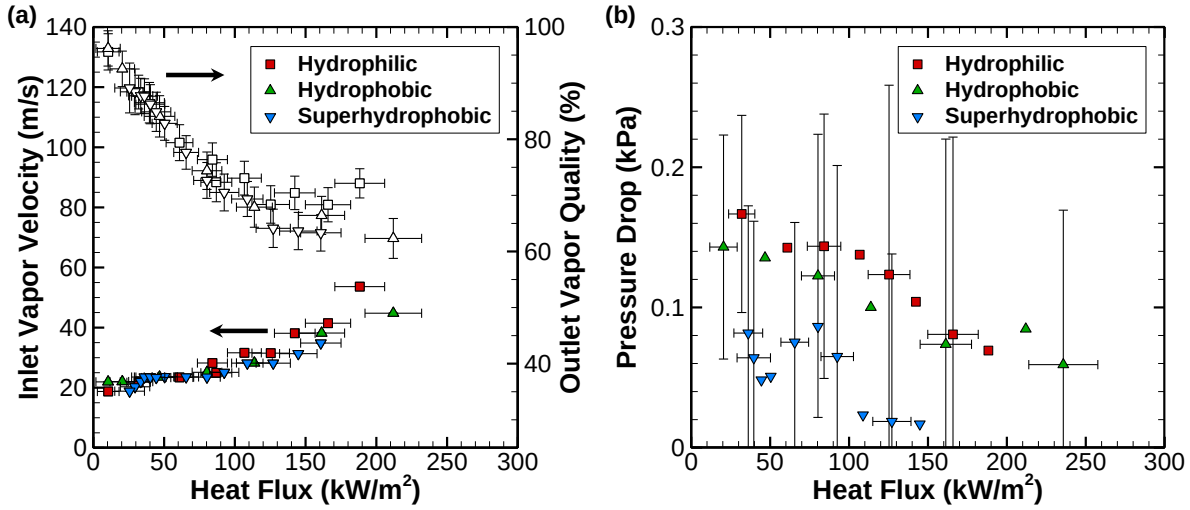


**Figure 4**: Steam conditions during the experiments: (a) test section inlet vapor velocity (left axis) and outlet vapor/steam quality (right axis) and (b) pressure drop of the vapor and condensate flow through the test section, for the different condensation modes corresponding to the hydrophilic, hydrophobic and superhydrophobic surfaces. For clarity, not all uncertainty bars are show in part (b).

The inlet vapor velocity and the outlet vapor quality are plotted in Figure 4a for different condensation modes and heat flux. At lower condensation heat flux and surface subcooling, the required steam valve opening (and $C_v$) was similar for the three condensation modes and tube samples tested, hence we observed similar inlet vapor velocity and the outlet vapor quality. At higher condensation heat flux, the experiments with the hydrophilic copper tube sample required a larger valve opening and resulted in higher inlet vapor velocity. However, the resulting estimation for the outlet vapor quality was within the experimental uncertainty for all

of the different modes. The outlet vapor quality for all tube samples tested decreased with increasing condensation heat flux.

Pressure drop for flow (vapor and condensate) through the condenser tube sample is plotted in Figure 4b for the various test conditions. The pressure drop over the entire length of the condenser tube ($L_{tube}$ ≈19 cm) sample was <200 Pa for all conditions and tube samples tested. While measured pressure drop values were within measurement uncertainty, two keys trends were observed: (i) the pressure drop for the superhydrophobic tube sample (jumping droplet and flooded modes) was lower than the corresponding pressure drops for the hydrophilic (filmwise) and hydrophobic (dropwise) tube samples, and (ii) the pressure drop decreased with increasing heat flux. The pressure drop during filmwise condensation was the highest, though a similar pressure drop was observed for dropwise condensation on the hydrophobic surface. The lowest pressure drop was measured for the superhydrophobic surface during the jumping droplet mode. We attribute the reason to be that the small droplets (<100 μm) jumping off the condenser surface were entrained in the vapor flow and therefore had a small contribution to the overall pressure drop. However, the mechanism facilitating a low pressure drop during the flooded mode is not known and requires more investigation in the future. The pressure drop also decreased as the condensation heat flux increased, despite an inlet vapor velocity increase (larger steam valve opening). This counterintuitive behavior was due to the decrease in the vapor quality as the condensation heat flux increased, which decelerated the flow as it changed phase from vapor to liquid along the condenser length. The deceleration that resulted from phase-change has a greater influence on the pressure drop than the increased inlet vapor velocity based on widely applied two-phase pressure drop models [36]. For a fixed surface subcooling, higher condensation rates resulted in lower vapor quality and pressure drop during the jumping droplet and dropwise condensation regimes as compared to the filmwise mode.

In typical ACCs used in steam power plants, the condensation heat flux is on the order of ≈40-50 kW/m$^2$ [3]. Based on our experimental measurements in this range, the jumping droplet condensation mode had the highest condensation HTC ≈66 kW/m$^2$·K as compared to the dropwise (≈43 kW/m$^2$·K) and filmwise (≈27 kW/m$^2$·K) modes. Additionally, the reduced pressure drop through the condenser tube offers an additional benefit to leveraging the jumping droplet mode over traditional filmwise and dropwise condensation modes. However, despite the enhancements in heat transfer and pressure drop characteristics, a key concern with any low surface energy coating used to promote enhanced dropwise condensation is the coating durability during extended periods of condensation. The nanostructures are known to be robust

in steam and condensation environments (<100 °C), however, coating robustness must be improved [37]. Harnessing the jumping droplet mode to enhance condensation heat transfer in industrial applications requires thin (<50 nm) and robust coatings which are currently not available commercially. Here we have demonstrated the viability of the jumping droplet condensation mode in internal vapor flows when such robust coatings become available.

## 4. Conclusions

We report heat transfer and pressure drop performance during condensation of water vapor inside tubes in the presence of forced vapor flow for filmwise, dropwise and jumping droplet condensation on hydrophilic, hydrophobic and superhydrophobic condenser tube samples, respectively. The experiments were performed in a custom built closed system test setup and the operating conditions were set to simulate typical steam condensation conditions in industrial ACCs.

The experimental measurements showed that the jumping droplet mode of condensation had the highest condensation HTC (≈68 kW/m$^2$·K) at a condensation heat flux ≈50 kW/m$^2$. However, beyond this heat flux, the supersaturation was higher than the critical value for the CuO nanostructure, and the surface began to flood. The condensation HTC in this flooded mode of condensation, where the droplets were pinned to the surface and the droplet departure size increased, was ≈26 kW/m$^2$·K. Dropwise condensation had a maximum condensation HTC (≈65 kW/m$^2$·K) above ≈250 kW/m$^2$, and the HTC was dependent on the vapor velocity. This dependence on vapor velocity had been observed in prior work with traditional dropwise condensation (non-jumping droplets) on superhydrophobic surfaces. Filmwise condensation had the lowest condensation HTC (≈23 kW/m$^2$·K) due to the presence, and corresponding thermal resistance, of the condensate film on the condenser surface. The lowest pressure drop measurements were recorded for the superhydrophobic surface, though all measurements were within the experimental uncertainty. Finally, we observed that the pressure drop decreased at higher condensation heat flux and we attributed this effect to the decrease in vapor quality as the heat flux increases.

While the results we present here show potential, thin hydrophobic coating durability is a key concern that will need to be addressed before this technology (or any dropwise condensation technology) is adopted in industrial scale commercial applications [38, 39]. Additionally, future work will focus on imaging the jumping droplet behavior in internal forced convective vapor flow, which was not possible with the current setup. These visualizations will offer

additional insight into: the transition to flooding with increased heat flux (and surface subcooling), the effect of vapor flow shear on droplet removal in both the flooded and jumping droplet regimes, the occurrence of multi-hop jumping droplet events (*i.e.*, jumping droplets return to the surface and promote additional jumping events by coalescing with existing droplets on the surface) and how they affect heat transfer or flooding behavior, interacting jumping droplets in the vapor flow, and the mechanism for the decreased pressure drop in the flooded mode (in addition to mass flow deceleration effects). Furthermore, in addition to flow visualizations, comprehensive modeling of the jumping droplet condensation mode [26] in internal vapor flows [27] is required to elucidate key mechanisms (*e.g.*, reduced pressure drop due to droplet entrainment, multi-hop events, *etc.*) that promote pressure drop and condensation heat transfer enhancements. With these future considerations in mind, our work demonstrated the viability of the jumping droplet mode of condensation to enhance condensation performance and reduce pressure drop in industrial condensers, thermal management devices (*e.g.*, vapor chambers), water harvesting, and thermal water desalination technologies.

## 6. Acknowledgments

The authors acknowledge funding for this research from the Electric Power Research Institute (EPRI) under award number 00-10002062, with Dr. Jessica Shi as Program Manager. The authors also acknowledge support from the Office of Naval Research (ONR) with Dr. Mark Spector as program manager. D.J.P. acknowledges funding received by the National Science Foundation Graduate Research Fellowship under Grant No. 1122374. Any opinion, findings, conclusions, or recommendations expressed in this material are those of the authors and do not necessarily reflect the views of the National Science Foundation.

## Appendix

**A.** Steady state operation data

The time to achieve steady state operation was typically 8-10 minutes, data was recorded for 4 minutes after steady state was achieved, and the data analysis was performed with measurement data averaged over 3 minutes. A typical sample of the steady state data (≈3 minutes) is shown below in Figure A1.

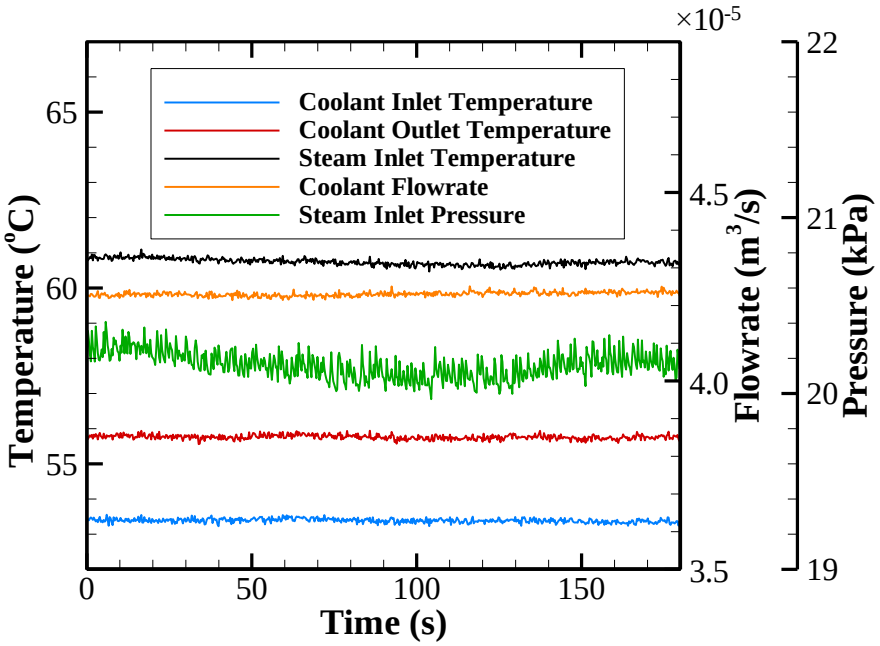


**Figure A1**: Raw measurement data for temperature (coolant inlet and outlet, and steam inlet), volumetric flowrate and pressure (steam inlet) at steady state for a typical experiment; the measurement conditions for this data correspond to $q''$ ≈84 kW/m$^2$, $\Delta T_{LM}$ ≈5.7 °C.

**B.** Uncertainty estimation

We performed standard uncertainty estimation [40] for the independent measurements ($T$, P and $\dot{V}$) and the derived quantities ($q''$, $\bar{U}$, *etc.*) *via* error propagation of the fundamental voltage measurement uncertainty, standard deviation of temporal measurements and calibration uncertainty. Here we briefly outline the various uncertainty calculations where $w$ is the variable used to describe uncertainty in the measurement of any parameter.

The uncertainty in the measurements of the independent parameters, temperature $T$, pressure $P$ and volumetric flowrate $\dot{V}$ are:

$$w_T = \left[ \left(T_{UNC}\right)^2 + \left(T_{STD}\right)^2 + \left(T_{DAQ}\right)^2 \right]^{1/2} \quad \text{(B1)}$$

$$w_{\mathrm{P}} = \left[ \left( P_{\mathrm{UNC}} \right)^2 + \left( P_{\mathrm{STD}} \right)^2 + \left( P_{\mathrm{DAQ}} \right)^2 \right]^{1/2} \tag{B2}$$

$$w_{\dot{\mathrm{V}}} = \left[ \left( \dot{V}_{\mathrm{UNC}} \right)^2 + \left( \dot{V}_{\mathrm{STD}} \right)^2 + \left( \dot{V}_{\mathrm{DAQ}} \right)^2 \right]^{1/2} \tag{B3}$$

In the above expressions for the uncertainties, the subscripts UNC, STD and DAQ refer to the device accuracy (or calibration uncertainty/accuracy), one standard deviation of the temporal data (averaged over ≈180 s) and the data acquisition card uncertainty, respectively. These uncertainties for the independent parameters apply to all the following uncertainties for the derived quantities where the independent parameters correspond to the specific measurements, *e.g.*, inlet, outlet, vapor, *etc.* Table B1 lists the nominal UNC and DAQ values for each measured quantity.

**Table B1**: Measurement uncertainties from calibration of the device/transducer (UNC) and the data acquisition card (DAQ) for fundamental measured parameters

| **Measurement Type** | **Uncertainty** |
|---|---|
| Temperature (Thermocouple, J-Type)†, K | 0.1 |
| Temperature (DAQ)†, K | 0 |
| Pressure (Transducer), kPa | 0.028 |
| Pressure (DAQ)‡, kPa | 0.0021 |
| Volumetric Flowrate (Flowmeter), $m^3/s$ | $3\times10^{-6}$ |
| Volumetric Flowrate (DAQ)‡, $m^3/s$ | $1\times10^{-8}$ |
| Convection Correlation (Gnielinski), % | 5 |

† After calibration

‡ Converted to appropriate units from DAQ voltage uncertainty

The following equations correspond to the uncertainties of the various derived quantities and each equation identifies the equation for the derived quantity and the corresponding measurement uncertainty:

$$\Delta T_{\mathrm{flow}} = T_{\mathrm{out}} - T_{\mathrm{in}}$$

$$w_{\Delta T_{\mathrm{flow}}} = \left\{ \left[ \frac{\partial \left( \Delta T_{\mathrm{flow}} \right)}{\partial T_{\mathrm{out}}} \cdot w_{T_{\mathrm{out}}} \right]^2 + \left[ \frac{\partial \left( \Delta T_{\mathrm{flow}} \right)}{\partial T_{\mathrm{in}}} \cdot w_{T_{\mathrm{in}}} \right]^2 \right\}^{1/2} \tag{B4}$$

$$\Delta T_{\mathrm{LM}} = \frac{\left(T_{\mathrm{vap}} - T_{\mathrm{in}}\right) - \left(T_{\mathrm{vap}} - T_{\mathrm{out}}\right)}{\ln\left[\frac{\left(T_{\mathrm{vap}} - T_{\mathrm{in}}\right)}{\left(T_{\mathrm{vap}} - T_{\mathrm{out}}\right)}\right]}$$

$$w_{\Delta T_{\mathrm{LM}}} = \left\{\left[\frac{\partial\left(\Delta T_{\mathrm{LM}}\right)}{\partial T_{\mathrm{v}}} \cdot w_{T_{\mathrm{vap}}}\right]^2 + \left[\frac{\partial\left(\Delta T_{\mathrm{LM}}\right)}{\partial T_{\mathrm{in}}} \cdot w_{T_{\mathrm{in}}}\right]^2 + \left[\frac{\partial\left(\Delta T_{\mathrm{LM}}\right)}{\partial T_{\mathrm{out}}} \cdot w_{T_{\mathrm{out}}}\right]^2\right\}^{1/2} \tag{B5}$$

$$\Delta P_{\mathrm{vap}} = P_{\mathrm{in}} - P_{\mathrm{out}}$$

$$w_{\Delta \mathrm{P}} = \left\{\left[\frac{\partial\left(\Delta P_{\mathrm{vap}}\right)}{\partial P_{\mathrm{in}}} \cdot w_{P_{\mathrm{in}}}\right]^2 + \left[\frac{\partial\left(\Delta P_{\mathrm{vap}}\right)}{\partial P_{\mathrm{out}}} \cdot w_{P_{\mathrm{out}}}\right]^2\right\}^{1/2} \tag{B6}$$

$$\dot{m}_{\mathrm{coolant}} = \rho_{\mathrm{coolant}} \cdot \dot{V}$$

$$w_{\dot{\mathrm{m}}} = \left\{\left[\frac{\partial\left(\dot{m}_{\mathrm{coolant}}\right)}{\partial \dot{V}} \cdot w_{\dot{\mathrm{V}}}\right]^2\right\}^{1/2} \tag{B7}$$

$$q'' = \frac{\dot{m}_{\mathrm{coolant}} \cdot c_{\mathrm{p}}}{A_{\mathrm{i}}}\left(\Delta T_{\mathrm{flow}}\right)$$

$$w_{\mathrm{q''}} = \left\{\left[\frac{\partial\left(q''\right)}{\partial \dot{m}_{\mathrm{coolant}}} \cdot w_{\dot{\mathrm{m}}_{\mathrm{coolant}}}\right]^2 + \left[\frac{\partial\left(q''\right)}{\partial T_{\mathrm{out}}} \cdot w_{T_{\mathrm{out}}}\right]^2 + \left[\frac{\partial\left(q''\right)}{\partial T_{\mathrm{in}}} \cdot w_{T_{\mathrm{in}}}\right]^2\right\}^{1/2} \tag{B8}$$

$$\mathrm{Re} = \frac{\rho_{\mathrm{coolant}} \cdot D_{\mathrm{h}}}{A \cdot \mu_{\mathrm{coolant}}} \cdot \dot{V}$$

$$w_{\mathrm{Re}} = \left\{\left[\frac{\partial\left(\mathrm{Re}\right)}{\partial \dot{V}} \cdot w_{\dot{\mathrm{V}}}\right]^2\right\}^{1/2} \tag{B9}$$

$$\bar{U} = \frac{q''}{\Delta T_{\mathrm{LM}}} = \frac{\rho_{\mathrm{coolant}} \cdot c_{\mathrm{p}} \cdot \dot{V}}{A_{\mathrm{i}}}\left(T_{\mathrm{out}} - T_{\mathrm{in}}\right) \cdot \frac{1}{\frac{\left(T_{\mathrm{vap}} - T_{\mathrm{in}}\right) - \left(T_{\mathrm{vap}} - T_{\mathrm{out}}\right)}{\ln\left[\frac{\left(T_{\mathrm{vap}} - T_{\mathrm{in}}\right)}{\left(T_{\mathrm{vap}} - T_{\mathrm{out}}\right)}\right]}} = \frac{\rho_{\mathrm{coolant}} \cdot c_{\mathrm{p}} \cdot \dot{V}}{A_{\mathrm{i}}} \cdot \ln\left[\frac{\left(T_{\mathrm{vap}} - T_{\mathrm{in}}\right)}{\left(T_{\mathrm{vap}} - T_{\mathrm{out}}\right)}\right] \tag{B10}$$

$$w_{\bar{\mathrm{U}}} = \left\{\left[\frac{\partial\left(\bar{U}\right)}{\partial \dot{V}} \cdot w_{\dot{\mathrm{V}}}\right]^2 + \left[\frac{\partial\left(\bar{U}\right)}{\partial T_{\mathrm{out}}} \cdot w_{T_{\mathrm{out}}}\right]^2 + \left[\frac{\partial\left(\bar{U}\right)}{\partial T_{\mathrm{in}}} \cdot w_{T_{\mathrm{in}}}\right]^2 + \left[\frac{\partial\left(\bar{U}\right)}{\partial T_{\mathrm{vap}}} \cdot w_{T_{\mathrm{vap}}}\right]^2\right\}^{1/2}$$

$$h_{\text{condensation}} = \left[ \frac{1}{\bar{U}} - \frac{A_i}{A_o \cdot h_{\text{convection}}} - \frac{1}{K_{\text{conduction}}} \right]^{-1}$$

$$K_{\text{conduction}} = \frac{2\pi \cdot L \cdot k_{\text{tube}}}{A_i \cdot \ln\left(d_{\text{OD}}/d_{\text{ID}}\right)} \tag{B11}$$

$$w_{h_{\text{condensation}}} = \left\{ \left[ \frac{\partial\left(h_{\text{condensation}}\right)}{\partial \bar{U}} \cdot w_{\bar{U}} \right]^2 + \left[ \frac{\partial\left(h_{\text{condensation}}\right)}{\partial h_{\text{convection}}} \cdot w_{h_{\text{convection}}} \right]^2 + \left[ \frac{\partial\left(h_{\text{condensation}}\right)}{\partial K_{\text{conduction}}} \cdot w_{K_{\text{conduction}}} \right]^2 \right\}^{1/2}$$

$$v_{\text{steam}} = 0.0002\left( \frac{C_v}{A_i} \sqrt{\frac{\rho_{\text{air}}}{\rho_{\text{vap}}}} \sqrt{\left(T_{\text{boiler-vap}} + 273.15\right)} \right)$$

$$w_{v_{\text{steam}}} = \left\{ \left[ \frac{\partial\left(v_{\text{steam}}\right)}{\partial T_{\text{boiler-vap}}} \cdot w_{T_{\text{boiler-vap}}} \right]^2 \right\}^{1/2} \tag{B12}$$

$$\dot{m}_{\text{vap-in}} = \rho_{\text{vap}} \cdot v_{\text{steam}} \cdot \left( \frac{\pi}{4} d_{\text{ID}}^2 \right)$$

$$w_{\dot{m}_{\text{vap-in}}} = \left\{ \left[ \frac{\partial\left(\dot{m}_{\text{vap-in}}\right)}{\partial v_{\text{steam}}} \cdot w_{v_{\text{steam}}} \right]^2 \right\}^{1/2} \tag{B13}$$

$$x = 1 - \frac{q'' \cdot A_i}{\dot{m}_{\text{vap-in}} \cdot h_{\text{fg}}}$$

$$w_x = \left\{ \left[ \frac{\partial(x)}{\partial q''} \cdot w_{q''} \right]^2 + \left[ \frac{\partial(x)}{\partial \dot{m}_{\text{vap-in}}} \cdot w_{\dot{m}_{\text{vap-in}}} \right]^2 \right\}^{1/2} \tag{B14}$$

**C.** Nucleation density and critical supersaturation for flooding

We predict the relative nucleation density/concentration for condensate nucleus formation from classical nucleation theory [34], as a function of both the condensing vapor temperature $T_{\text{vap}}$ and the surface contact angle $\theta$ for a fixed supersaturation of $S \approx 1.12$; the results are plotted in Figure C1. The general expression for this equilibrium cluster density is:

$$C^* = C_0 e^{\left(-W^*/k_B \cdot T_{\text{vap}}\right)} \tag{C1}$$

where, $k_B$ is the Boltzmann constant ($1.3806\times10^{-23}$ m$^2$·kg/s$^2$·K), $T_{\text{vap}}$ is the vapor condensation temperature, $C_0$ is the concentration of sites on the condenser surface on which clusters of the nucleating condensate can form and is typically independent of temperature for heterogeneous nucleation, and $W^*$ is the energy spent on the nucleus formation (*i.e.*, the nucleation work). For heterogeneous nucleation of cap-shaped clusters of a condensed phase, $W^*$ is given by:

$$W^* = \psi \frac{16\pi \cdot V_0^2 \gamma_{lv}^3}{3 \cdot \Delta\mu^2} \tag{C2}$$

where, $V_0$ is the water molecule volume ($3\times10^{-29}$ m$^3$), $\gamma_{lv}$ is the condensed phase surface tension, and $\psi$ is a numerical factor accounting for the wettability of the condenser surface given by:

$$\psi = \frac{1}{4}(2+\cos\theta)(1-\cos\theta)^2 \tag{C3}$$

where, $\theta$ is the contact angle in radian.

In eq. C2 above, $\Delta\mu$ is the thermodynamic driving force for the nucleation process:

$$\Delta\mu = k_B \cdot T_{vap} \cdot \ln(S) - V_0 \cdot \left(P_{sat\text{-}vap} - P_{sat\text{-}wall}\right) \tag{C4}$$

where, $P_{sat\text{-}vap}$ and $P_{sat\text{-}wall}$ are the saturation pressure of the condensing fluid at the vapor temperature and condenser surface temperature, respectively, and $S$ is the supersaturation which is the ratio of $P_{sat\text{-}vap}$ to $P_{sat\text{-}wall}$. All thermophysical properties have temperature dependent data from the NIST REFPROP database [41].

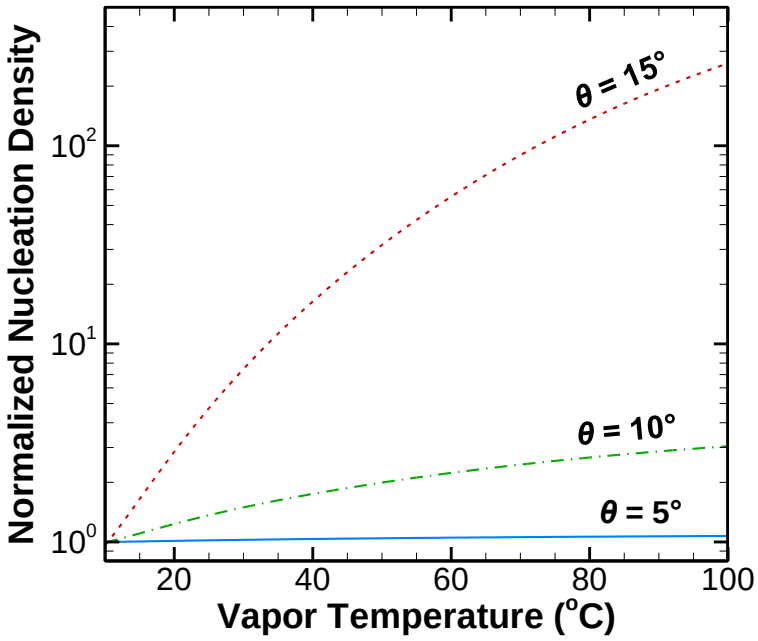


**Figure C1**: Normalized nucleation density for a supersaturation $S \approx 1.12$ at various vapor temperatures and for different substrate contact angle, as predicted from classical nucleation theory. Note that a superhydrophobic substrate requires a high surface energy (low contact angle) site for nucleation to occur at low supersaturation conditions [8].

In Figure C1, we plot the normalized nucleation density (normalized to the density at $T_{vap} \approx 10$ °C) as a function of vapor temperature and condenser surface contact angle. The data

is for a constant supersaturation of S ≈1.12. Based on literature [8, 31], we expect nucleation to occur at sites where the local energy barrier to nucleation is low, *i.e.*, at low contact angle hydrophilic defects. Hence for $\theta$ <10°, the expected change in nucleation density (which affects nucleation density mediated flooding onset) with temperature is less than a factor of 2. This supports the validity of the assumption of $S_{cr}$ ≈1.12 (from Miljkovic *et al.* [19]) for the current experimental data, discussion and analysis (Figure 2b) presented in the paper.

From a thermal resistance network (eq. 4, Figure C2a) which includes the condensation, thermal conduction and coolant forced convection resistances, we estimated the supersaturation $S$ for various combinations of the coolant to vapor temperature difference ($\Delta T$), condensation heat flux ($q$") and condensation heat transfer coefficient ($h_{condensation}$). The results are plotted in Figure C2b for a constant Reynolds number ≈4000 (average in experiments). Using the results from this model, we predict the criteria for the onset of flooding ($S_{cr}$ ≈1.12) outlined in Figure 2b by the shaded region.

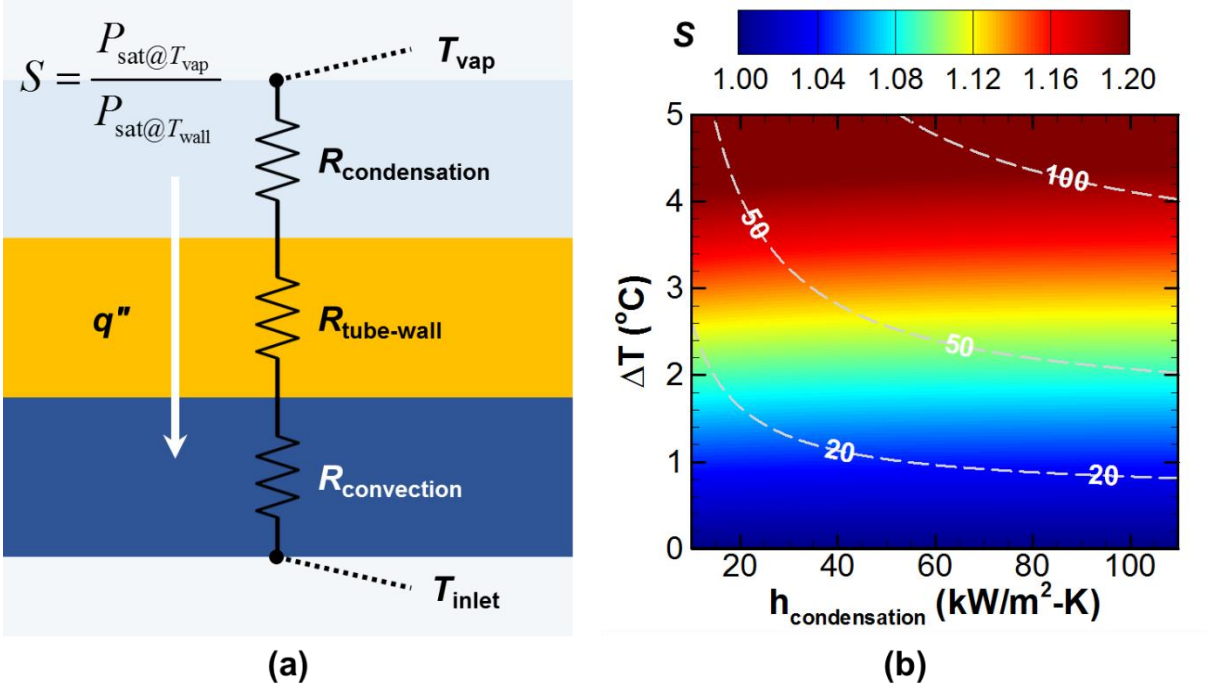


**Figure C2**: Local supersaturation from thermal resistance network for heat transfer from vapor to the coolant in the heat exchanger, (a) schematic of thermal resistance network, and (b) results from the model. Note that the dashed lines in (b) represent the local heat flux in kW/m$^2$.

## Statement of Competing Interest

The authors declare no competing interests.

## References

[1] R. Hankey, C. Cassar, J. Liu, P. Wong, O. Yildiz, Electric Power Monthly (with data for May 2018), U.S. Energy Information Administration (EIA), Washington, DC, 2018.
[2] H.D. Schilling, Prospects of power plant technology, VGB Kraftwerkstechnik, 73(8) (1993) 658 - 670.
[3] J.L. Tsou, J. Maulbetsch, J. Shi, Power Plant Cooling System Overview for Researchers and Technology Developers, Electric Power Reseach Institute (EPRI), Palo Alto, 2013.
[4] M.A. Maupin, J.F. Kenny, S.S. Hutson, J.K. Lovelace, N.L. Barber, K.S. Linsey, Estimated use of water in the United States in 2010, U.S. Geological Survey (USGS), Reston, VA, 2014.
[5] S.-Y. Pan, S.W. Snyder, A.I. Packman, Y.J. Lin, P.-C. Chiang, Cooling water use in thermoelectric power generation and its associated challenges for addressing water-energy nexus, Water-Energy Nexus, (2018).
[6] W. Nusselt, The surface condensation of water vapour., Zeitschrift Des Vereines Deutscher Ingenieure, 60 (1916) 541-546.
[7] J.W. Rose, Dropwise condensation theory and experiment: a review, Proceedings of the Institution of Mechanical Engineers Part a-Journal of Power and Energy, 216 (2002) 115-128.
[8] R. Enright, N. Miljkovic, A. Al-Obeidi, C.V. Thompson, E.N. Wang, Condensation on Superhydrophobic Surfaces: The Role of Local Energy Barriers and Structure Length Scale, Langmuir, 28(40) (2012) 14424-14432.
[9] N. Miljkovic, R. Enright, E.N. Wang, Effect of Droplet Morphology on Growth Dynamics and Heat Transfer during Condensation on Superhydrophobic Nanostructured Surfaces, ACS Nano, 6(2) (2012) 1776-1785.
[10] J.B. Boreyko, C.-H. Chen, Self-Propelled Dropwise Condensate on Superhydrophobic Surfaces, Physical Review Letters, 103(18) (2009) 184501.
[11] R. Enright, N. Miljkovic, J. Sprittles, K. Nolan, R. Mitchell, E.N. Wang, How Coalescing Droplets Jump, ACS Nano, 8(10) (2014) 10352-10362.
[12] F. Liu, G. Ghigliotti, J.J. Feng, C.-H. Chen, Numerical simulations of self-propelled jumping upon drop coalescence on non-wetting surfaces, Journal of Fluid Mechanics, 752 (2014) 39-65.
[13] J.B. Boreyko, C.-H. Chen, Self-propelled jumping drops on superhydrophobic surfaces, Physics of Fluids, 22(9) (2010) 091110.
[14] T. Mouterde, T.-V. Nguyen, H. Takahashi, C. Clanet, I. Shimoyama, D. Quéré, How merging droplets jump off a superhydrophobic surface: Measurements and model, Physical Review Fluids, 2(11) (2017) 112001.
[15] H. Cha, C. Xu, J. Sotelo, J.M. Chun, Y. Yokoyama, R. Enright, N. Miljkovic, Coalescence-induced nanodroplet jumping, Physical Review Fluids, 1(6) (2016) 064102.
[16] X. Gong, X. Gao, L. Jiang, Recent Progress in Bionic Condensate Microdrop Self-Propelling Surfaces, Advanced Materials, 29(45) (2017) 1703002.
[17] M. Kollera, U. Grigull, Über das Abspringen von Tropfen bei der Kondensation von Quecksilber (The bouncing off phenomenon of droplets with condensation of mercury), Wärme - und Stoffübertragung, 2(1) (1969) 31-35.
[18] N. Miljkovic, R. Enright, E.N. Wang, Modeling and Optimization of Superhydrophobic Condensation, Journal of Heat Transfer, 135(11) (2013) 111004-111004.
[19] N. Miljkovic, R. Enright, Y. Nam, K. Lopez, N. Dou, J. Sack, E.N. Wang, Jumping-Droplet-Enhanced Condensation on Scalable Superhydrophobic Nanostructured Surfaces, Nano Letters, 13(1) (2013) 179-187.

[20] J. Zhu, Y. Luo, J. Tian, J. Li, X. Gao, Clustered Ribbed-Nanoneedle Structured Copper Surfaces with High-Efficiency Dropwise Condensation Heat Transfer Performance, ACS Applied Materials & Interfaces, 7(20) (2015) 10660-10665.
[21] S. Jun Lee, S. Lee, K. Hyoung Kang, Droplet Jumping by Electrowetting and its Application to the Three-Dimensional Digital Microfluidics, Applied Physics Letters, 100(8) (2012) 081604-081604.
[22] B.B.Y.Z. Jonathan, C.-H. Chen, Planar jumping-drop thermal diodes, in, 2011.
[23] R. Wen, Q. Li, J. Wu, G. Wu, W. Wang, Y. Chen, X. Ma, D. Zhao, R. Yang, Hydrophobic copper nanowires for enhancing condensation heat transfer, Nano Energy, 33 (2017) 177-183.
[24] R. Wen, S. Xu, D. Zhao, Y.-C. Lee, X. Ma, R. Yang, Hierarchical Superhydrophobic Surfaces with Micropatterned Nanowire Arrays for High-Efficiency Jumping Droplet Condensation, ACS Applied Materials & Interfaces, 9(51) (2017) 44911-44921.
[25] R. Wen, S. Xu, X. Ma, Y.-C. Lee, R. Yang, Three-Dimensional Superhydrophobic Nanowire Networks for Enhancing Condensation Heat Transfer, Joule, 2(2) (2018) 269-279.
[26] Z. Xu, L. Zhang, K. Wilke, E.N. Wang, Multiscale Dynamic Growth and Energy Transport of Droplets during Condensation, Langmuir, 34(30) (2018) 9085-9095.
[27] P. Birbarah, N. Miljkovic, Internal convective jumping-droplet condensation in tubes, International Journal of Heat and Mass Transfer, 114 (2017) 1025-1036.
[28] K. Cheng, S. Kim, S. Lee, K.J. Kim, Internal dropwise condensation: Modeling and experimental framework for horizontal tube condensers, International Journal of Heat and Mass Transfer, 83 (2015) 99-108.
[29] D.E. Kim, H.S. Ahn, T.-S. Kwon, Experimental investigation of filmwise and dropwise condensation inside transparent circular tubes, Applied Thermal Engineering, 110 (2017) 412-423.
[30] D.J. Preston, N. Miljkovic, J. Sack, R. Enright, J. Queeney, E.N. Wang, Effect of hydrocarbon adsorption on the wettability of rare earth oxide ceramics, Applied Physics Letters, 105(1) (2014) 011601.
[31] R. Enright, N. Miljkovic, N. Dou, Y. Nam, E.N. Wang, Condensation on Superhydrophobic Copper Oxide Nanostructures, Journal of Heat Transfer, 135(9) (2013) 091304-091304.
[32] X.-H. Ma, X.-D. Zhou, Z. Lan, Y.-M. Li, Y. Zhang, Condensation heat transfer enhancement in the presence of non-condensable gas using the interfacial effect of dropwise condensation, International Journal of Heat and Mass Transfer, 51(7–8) (2008) 1728-1737.
[33] J.H. Lienhard IV, J.H. Lienhard V, A Heat Transfer Textbook, 3rd ed., Phlogiston Press, 2002.
[34] D. Kaschiev, Nucleation: Basic Theory With Applications, Butterworth Heinemann, Oxford, 2000.
[35] D. Torresin, M.K. Tiwari, D. Del Col, D. Poulikakos, Flow Condensation on Copper-Based Nanotextured Superhydrophobic Surfaces, Langmuir, 29(2) (2012) 840-848.
[36] V.P. Carey, Liquid-Vapor Phase-Change Pheomena, 2nd ed., Taylor & Francis, New York, 2008.
[37] J.H. Sack, Fabrication and Robustness Testing of Superhydrophobic Nanostructured Surfaces for Enhanced Jumping Condensation, M.S., Massachusetts Institute of Technology, Cambridge, MA, 2015.
[38] A.T. Paxson, J.L. Yagüe, K.K. Gleason, K.K. Varanasi, Stable Dropwise Condensation for Enhancing Heat Transfer via the Initiated Chemical Vapor Deposition (iCVD) of Grafted Polymer Films, Advanced Materials, 26(3) (2013) 418-423.
[39] D.J. Preston, D.L. Mafra, N. Miljkovic, J. Kong, E.N. Wang, Scalable Graphene Coatings for Enhanced Condensation Heat Transfer, Nano Letters, 15(5) (2015) 2902-2909.
[40] J.P. Holman, Experimental methods for engineers, 7th ed., McGraw-Hill, Boston, 2001.

[41] E.W. Lemmon, I.H. Bell, M.L. Huber, M.O. McLinden, REFPROP- Standard Reference Data Program, in, National Institute of Standards and Technology (NIST), Gaithersburg, MD, 2018.